

LETTER TO THE EDITOR

Flavours in the box of chocolates: chemical abundances of kinematic substructures in the nearby stellar halo

Jovan Veljanoski¹ and Amina Helmi¹

Kapteyn Astronomical Institute, University of Groningen, Landleven 12, 9747 AD Groningen, The Netherlands
e-mail: jovan@astro.rug.nl

March 9, 2024

ABSTRACT

Context. Stellar halos contain tracers of the assembly history of massive galaxies like our own. Exploiting the synergy between the TGAS and the spectroscopic RAVE surveys, Helmi et al. (2017) recently discovered several distinct substructures in the Solar neighbourhood, defined in integrals of motion space. Some of these substructures may be examples of the building blocks that built up the stellar halo.

Aims. We analyse the chemical properties of stars in these substructures, with focus on their iron and α -element abundances as provided by the RAVE survey chemical pipeline.

Methods. We perform comparisons of the $[\text{Fe}/\text{H}]$ and $[\text{Mg}/\text{Fe}]$ distributions of the substructures to that of the entire halo sample defined in the TGAS×RAVE dataset.

Results. We find that over half of the nine substructures have $\sigma_{[\text{Fe}/\text{H}]} \leq 0.3$ dex. Two of the substructures have $\sigma_{[\text{Fe}/\text{H}]} \leq 0.1$ dex, which makes them possible remnants of disrupted globular clusters. As expected most substructures and the vast majority of our stellar halo sample are α -enhanced. Only one substructure shows a $[\text{Mg}/\text{Fe}]$ vs $[\text{Fe}/\text{H}]$ abundance trend distinct from the rest of the halo stars in our sample.

Key words. Galaxy: kinematics and dynamics – Galaxy: halo – Solar neighbourhood – abundances

1. Introduction

In the current cosmological model, much of the mass in galaxies similar to the Milky Way is assembled hierarchically: pre-galactic fragments coalesce to form larger objects. A by-product of this process is the formation of extended, diffuse stellar halos surrounding their host galaxies. Stellar halos thus keep a record of the accretion and merger events that happened from the onset of the assembly process in the early Universe, all the way to the present day. Indeed, wide-field Galactic surveys such as SDSS and PanSTARRS have revealed much substructure in the form of spatially coherent stellar streams (e.g. Belokurov et al. 2006; Bernard et al. 2014, 2016) in the outskirts of the Milky Way. Their findings are consistent with the idea that the outer stellar halo is predominantly, if not solely built via mergers.

In contrast, little is known about the assembly process of the inner stellar halo, and what fraction of it is composed by stellar streams. Using kinematic and metallicity data of stars in the extended Solar neighbourhood, Carollo et al. (2007, 2010) found those less bound to be on average on retrograde orbits and to be more metal-poor in comparison to inner halo stars, which on average have slightly prograde motions. This led to the idea of a two- component halo, where the inner parts would have predominantly formed *in situ* while the outer regions via accretion. This dual formation path of the Galactic stellar halo is partly supported by hydrodynamical simulations (e.g. Zolotov et al. 2009; Tissera et al. 2014), where the relative importance of the two channels can vary strongly depending on the cosmological history of the galaxy.

Conversely, if the stellar halo was fully built by accretion, models predict that over 300 streams should cross the Solar

neighbourhood (Helmi & White 1999; Helmi et al. 2003), and the first such streams were discovered nearly two decades ago (Helmi et al. 1999). Due to the shorter dynamical time-scales, the inner stellar halo is spatially well mixed however, causing the velocities of the stars in any substructure to become more clustered. Thus, the halo's granularity can only be discerned in large samples with accurate kinematics.

The launch of the *Gaia* satellite puts us in an unprecedented position to study the properties of stellar halo of the Milky Way. The first *Gaia* Data Release (DR1) provides the positions, parallaxes, proper motions, and mean *G*-band magnitudes for over 2 million stars in common with the *Tycho-II* and HIPPARCOS catalogues, in what is referred to as the *Tycho- Gaia* Astrometric Solution (TGAS, Gaia Collaboration et al. 2016; Lindegren et al. 2016).

Recently, Helmi et al. (2017, H17 hereafter) exploited the synergy between the TGAS and the spectroscopic RAVE surveys (DR5, Kunder et al. 2017) to select a sample of over 1000 halo stars using kinematics and metallicity criteria. Analysing the velocities of the stars in this sample by means of a correlation function, H17 found that the stellar halo near the Sun is consistent with being fully formed by accretion. In addition, these authors identified 10 distinct, statistically significant substructures in integrals of motion space.

These previously unknown substructures are the focus of this paper. Here we analyse the chemical composition of their constituent stars using the abundances available through the public RAVE DR5 catalogue. With the goal of learning more about their possible nature, this study is also a proof-of-concept of the chemical labelling/tagging ideas put forward by Freeman & Bland-

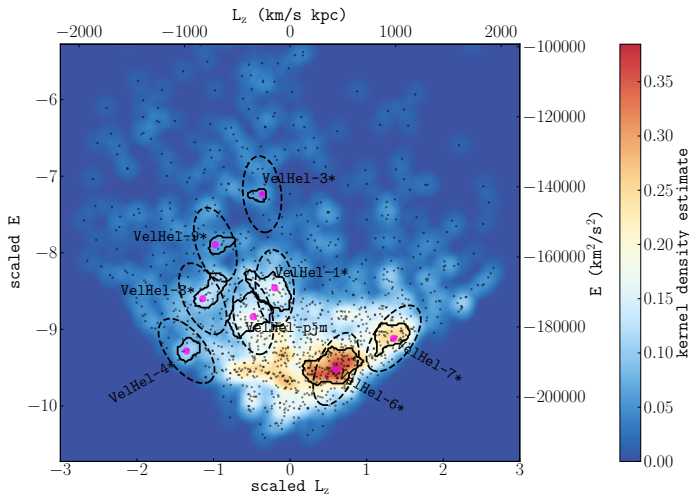


Fig. 1. Kernel density estimate of the distribution in $E - L_z$ for our sample of halo stars in the Solar neighbourhood. The individual stars are shown as black dots. The magenta points denote the statistically significant over-densities. The black contours mark the extent of these substructures, as determined by the watershed algorithm. The ellipses show the extended selection reported in Sec. 3.2. The naming of the structures follows the same convention as in H17.

Hawthorn (2002). For instance, if some of the substructures are remnants of disrupted globular clusters, their stars are expected to be α -enhanced with a very tight, even negligible spread in iron abundance.

This paper is structured as follows. In the next section we revisit the halo sample and the integrals of motion substructures of H17 by taking advantage of the improved parallaxes and metallicities derived by McMillan et al. (2017) for the TGAS×RAVE dataset. In Section 3 we analyse the abundances of the substructures, and summarise our findings in Section 4.

2. “A box full of chocolates” revisited

We start by redefining the halo substructures initially reported in H17, by using the dataset constructed by McMillan et al. (2017). These authors use the TGAS parallaxes as priors when computing the spectrophotometric parallaxes for stars in common between TGAS and RAVE. With this method the estimated distances have uncertainties on average two times smaller than their RAVE-only counterparts, and 1.4 times smaller than the corresponding TGAS uncertainties. With their method McMillan et al. (2017) also provide updated and more reliable $\log(g)$, T_{eff} and $[M/H]$ estimates.

We define the sample of halo stars following the steps taken by H17 (see their Sec. 2), using the TGAS×RAVE catalogue provided by McMillan et al. (2017). After applying several quality cuts¹, and a metallicity criterion $[M/H] \leq -1$ dex, we find 1823 tentative halo stars. In this work we use the “calibrated” metallicity estimates provided by McMillan et al. (2017). We then remove stars with (thick) disk-like kinematics as in H17, by fitting two multivariate Gaussians, and by retaining only those stars that have a higher probability of being drawn from the Gaussian component with the lowest rotational motion (in our case, this has a

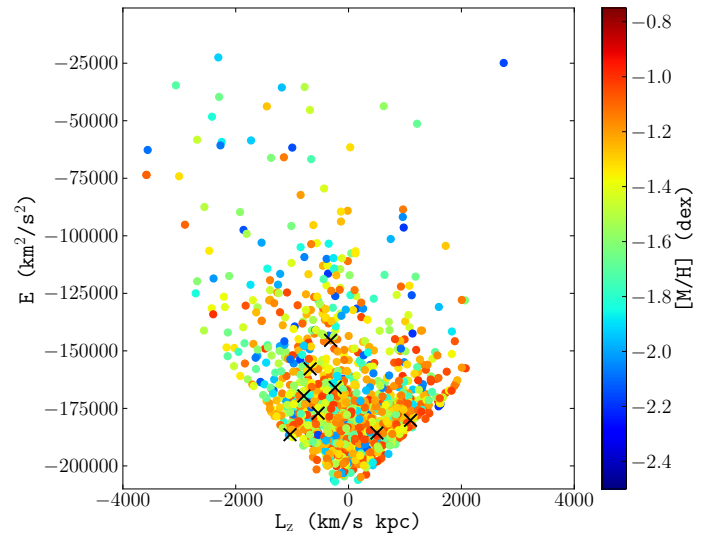


Fig. 2. Distribution of stars in our sample colour-coded by the RAVE metallicity $[M/H]$. The black crosses indicate the location of the over-densities identified in Fig. 1.

mean $v_y \approx -15 \text{ km s}^{-1}$). With this approach, we find 1217 high confidence, metal-poor halo stars.

With this updated sample we proceed to re-analyse their distribution in integrals of motion space: $E - L_z$. Fig. 1 shows this distribution for the more bound stars in this halo sample (i.e. those that satisfy $-21 \times 10^4 \leq E \leq -10 \times 10^4 \text{ km}^2 \text{ s}^{-2}$ and $-2000 \leq L_z \leq 2000 \text{ km s}^{-1} \text{ kpc}$).

To pick out any substructures that may be significant in this space, we proceed again as in H17. We first determined the density field (shown in Fig. 1), then applied a maximum filter to pick out over-densities, and then established which were statistically significant by comparison to randomised datasets obtained by reshuffling two velocity components. In this way we identify 8 over-densities marked by the magenta points on Fig. 1. Finally, we employ the watershed algorithm (Vincent & Soille 1991) to loosely determine the extent of the over-densities and thus their constituent stars.

Fig. 1, shows that we have recovered all but one of the substructures initially reported by H17 (see their Figure 10). Since not exactly the same stars are found in the substructures as in H17 (there is typically 60% overlap), we added an asterisk at the end of their H17 labels. The one structure that is not recovered, dubbed VelHel-5, can be visually identified in our data, but does not pass the significance tests, although a new structure appears that contains some stars from the original VelHel-1 and VelHel-5, which we label VelHel-pjm. We also do not recover the metal-poor tail of the disk because, in contrast to H17, we completely removed the disk stars during the Gaussian decomposition phase. Overall, the above procedure adds more validity to the structures discovered by H17, and makes us appreciate how robust results can be to small changes in the data.

In addition to the discoveries of the substructures in integrals of motion space, H17 also found that the stars with binding energies smaller than that of the Sun have preferentially retrograde orbits. We confirmed this result with our updated halo sample: 77% of the stars with $E > -13 \times 10^4 \text{ km}^2 \text{ s}^{-2}$ are on retrograde orbits. We also include this low binding energy retrograde component in our abundance analysis.

Fig. 2 shows the distribution of halo stars in the integrals of motion space, colour-coded by the value of their metallicity. We

¹ including a relative parallax uncertainties $\Delta\varpi/\varpi \leq 30\%$, where this can be the updated RAVE or TGAS-only parallaxes depending on which measurement has a smaller relative error, provided that the TGAS parallax is positive.

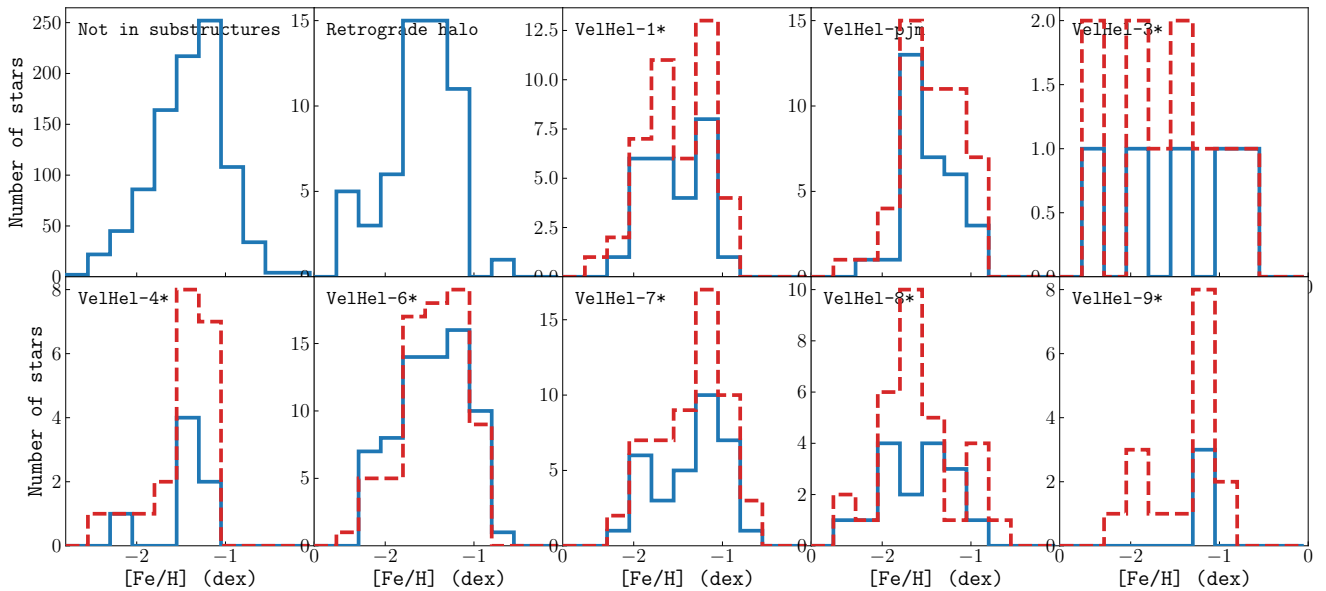


Fig. 3. The $[\text{Fe}/\text{H}]$ distributions of the stars in the statistically significant substructures identified in E - L_z space, including the retrograde halo. The blue solid histograms cover the stars identified using the watershed algorithm, while those in red correspond to the extended elliptical selection. The bins of all histograms have a constant width of 0.25 dex, which is the typical $[\text{Fe}/\text{H}]$ uncertainty.

can see that the stars with high binding energy are, on average, more metal-rich, while those in the less bound highly retrograde component appear to be somewhat more metal-poor, albeit with large scatter. This would thus be in agreement with the results of Carollo et al. (2007), although the “outer halo” component in our dataset is much more prominently retrograde.

3. Abundance analysis

The nominal RAVE DR5 data release provides abundances of a few iron peak elements (Fe, Ni), as well as several α -elements (Mg, Si, Ti). These abundances were derived with a pipeline first introduced for the third data release of RAVE (Boechse et al. 2011), and subsequently improved in later releases. The typical abundance is ~ 0.2 dex, and can increase slightly for $S/N < 40$. In addition, the RAVE DR5 stars have a mean $S/N = 55$ and a resolving power $R = \lambda/\Delta\lambda \sim 7500$.

Note that we do not use the abundance elements provided by *The Cannon* pipeline because the training set used is sparse in the regime of low metallicity giants and hence not reliable.

3.1. $[\text{Fe}/\text{H}]$ and α abundances

Figure 3 shows the $[\text{Fe}/\text{H}]$ distributions for the stars that comprise the statistically significant substructures identified in Section 2, as well as for the retrograde outer halo. One can see that substructures VelHel-4*, VelHel-pjm, VelHel-9*, and even the retrograde halo have pronounced peaks in their $[\text{Fe}/\text{H}]$ distributions, and relatively small dispersions.

We now examine whether the small spread of $[\text{Fe}/\text{H}]$ exhibited by the substructures is genuine, which would separate them from the overall halo sample judging by their iron abundances alone, or whether their observed $[\text{Fe}/\text{H}]$ distributions are simply chance occurrences. To quantify this we do the following test. We draw 10000 random sets of stars from the entire halo sample. Each random set contains as many stars as the substructure that is being examined. We then count how often a random set

has a smaller $[\text{Fe}/\text{H}]$ spread² compared to what is observed in the actual substructures.

The results from this test are listed in Table 1. From the second column of this Table we see that 5 out of the 9 substructures we are investigating, including the retrograde halo, have $[\text{Fe}/\text{H}]$ spreads of 0.3 dex or less. This is a rather small value given the typical abundance uncertainties are 0.25 dex. For substructures VelHel-4*, VelHel-pjm* and the retrograde halo, we see that the probability of observing distributions with such small spread by randomly selecting stars is $\sim 1\%$. Substructure VelHel-9* has the smallest $[\text{Fe}/\text{H}]$ spread amongst the substructures, but this quantity was measured only from 3 stars, and such a configuration happens 6% of the time in our random realisations.

Both Mg and Si are α -elements and their abundance is available for the largest fraction of stars that comprise our substructures. In Fig. 4 we show the $[\text{Mg}/\text{Fe}]$ as a function of $[\text{Fe}/\text{H}]$ ($[\text{Si}/\text{Fe}]$ follows a similar distribution). One can see that almost all substructures appear to be α -enhanced. The only exception is substructure VelHel-3*, but this result is still tentative at best, given that only 3 have Mg (and 4 stars have Si) abundance estimates. This is intriguing (given the Nissen & Schuster 2010, low- α sequence), and a K-S test that compares the cumulative distribution of the “smooth” stellar halo sample to that of VelHel-3* confirms this: we find a p -value < 0.01 .

3.2. Enlarged membership selection

One of the biggest challenges we are currently facing while trying to detect and characterise spatially mixed substructures in the Solar neighbourhood is the small number of halo stars that are available to us for analysis. In fact, the main reason why examining integrals of motion diagrams is so beneficial, is because we are effectively folding the 6-dimensional phase-space information into two dimensions, thus increasing the clustering

² What we refer to as “spread” is the difference between the values of the distribution at the 16th and the 84th percentile, divided by two. This is equivalent to one standard deviation in the case of a Gaussian distribution.

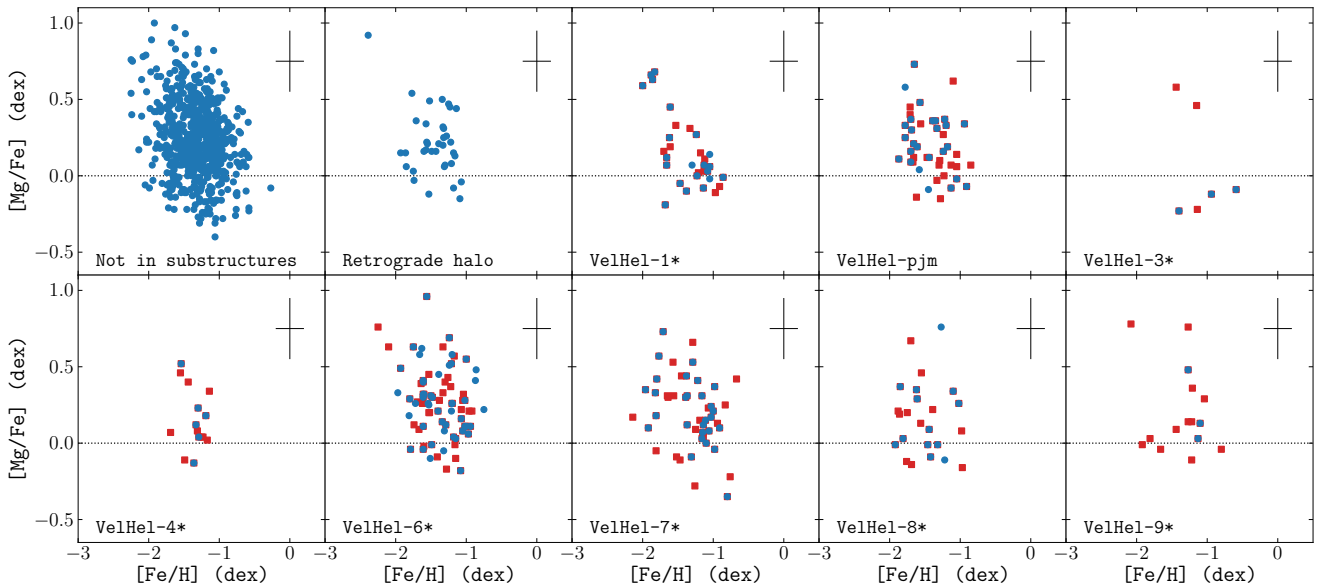


Fig. 4. $[\text{Fe}/\text{H}]$ vs $[\text{Mg}/\text{Fe}]$ (top) for the stars in the substructures, the retrograde halo, and the rest of the halo sample. The colour-coding is the same as in Fig. 3. One can see that the stars in most of the substructures follow a similar distribution as most of the stellar halo sample (except for those in VelHel-3*).

Table 1. The standard deviations of the $[\text{Fe}/\text{H}]$ distributions of the E - L_z substructures and the less-bound retrograde halo. The table also shows the frequency of observing a spread as small or smaller in the 10000 randomly drawn sets from the full halo dataset (see main text for details).

Substructure	Density selection		Elliptical selection	
	$\sigma_{[\text{Fe}/\text{H}]}$ (dex)	$P_{[\text{Fe}/\text{H}]}$ (%)	$\sigma_{[\text{Fe}/\text{H}]}$ (dex)	$P_{[\text{Fe}/\text{H}]}$ (%)
VelHel-1*	0.4	66	0.4	51
VelHel-3*	0.7	99	0.5	90
VelHel-4*	0.1	< 1	0.2	< 1
VelHel-6*	0.4	28	0.3	1
VelHel-7*	0.4	63	0.2	< 1
VelHel-8*	0.3	44	0.4	61
VelHel-9*	0.1	6	0.1	< 1
VelHel-pjm	0.2	2	0.3	2
retr. halo	0.3	1.2

an object exhibits in an E - L_z space for example, as we show on Figure 1. As described in Section 2, we detected the substructures analysed in this paper as over-densities in E - L_z space. The members of each structure were determined with the watershed algorithm that traces the density contour at some level of each structure. However, when the number of members is small, the extent and shape of a structure in E - L_z space is likely not well defined. From simulations of spatially mixed substructures in the Solar neighbourhood, we know that in E - L_z space they have regular, almost elliptical shapes with a small dispersion in L_z , while they can be quite elongated in energy, depending on the orbit and mass of the progenitor system (see e.g. Figure 6 in Helmi & de Zeeuw 2000). Thus it is possible that other members of the substructures are present in the E - L_z diagrams on Fig. 1, but they are not selected simply due to the shape of the underlying density field in the regime of low number statistics.

We thus attempt to analyse the elemental abundances of the substructures by selecting all stars that fall within an ellipse centred on the peak of the over-density identified in E -

L_z space, with a semi-major axis of 0.5 in scaled units of energy, and a semi-major axis of 0.25 in scaled units of L_z (since $\Delta E/E \propto 2\Delta L_z/L_z$), as shown in Fig. 1. The major axes of the ellipses are aligned with the line connecting the density peak of the substructures and the point of origin. Such a selection should approximate the shape that a substructure is expected to have in E - L_z in the presence of significantly more members. We proceed to re-examine the Fe and α -element abundance distributions of the substructures when their members are determined with this elliptical selection.

The red dashed histograms in Figure 3 show that adding more potential members to the substructures with the elliptical selection enhances the features seen in the original $[\text{Fe}/\text{H}]$ distributions. The most striking example is substructure VelHel-9*, in which the tentative peak observed with the nominal density selection is significantly enhanced: it now features 8 stars with a dispersion smaller than 0.1 dex.

This simple exercise shows that, there are potentially several stars that are likely members of the substructures which were not included via the original watershed-based criteria. If this were not the case, we would expect adding random stars to the substructures to smear out, and not improve, the features seen in their $[\text{Fe}/\text{H}]$ distributions. To quantify this, we repeat the statistical test we conducted in Section 3.1, now considering the additional stars. The last two columns in Table 1 indeed show that the increased prominence of the peaks makes the $[\text{Fe}/\text{H}]$ distributions for most of the structures less likely to be drawn by chance from the overall halo sample. On the other hand, the elliptical membership selection does not significantly change the distribution of stars in $[\text{Mg}/\text{Fe}]$ vs $[\text{Fe}/\text{H}]$ in our substructures, as shown in Fig. 4.

4. Summary

In this paper we examined the iron and α -element abundance distributions of the substructures originally identified in integrals of motions space by Helmi et al. (2017) in the Solar neighbourhood, searching for hints of their origin.

We started by defining a metal-poor halo sample following the steps described in Helmi et al. (2017) using the cross-match between the TGAS and RAVE catalogues with the updated spectrophotometric distances provided by McMillan et al. (2017). With this procedure we selected 1217 high confidence metal-poor halo stars. Using this data, we redefined the substructures originally discovered by Helmi et al. (2017) in E - L_z space. We recover all substructures (with at least 60% overlap in terms of membership) except for one, which is found to be less statistically significant.

We proceeded to analyse the Fe and Mg abundances available in RAVE DR5 for stars in the substructures, as well as for the retrograde halo stars that have $E > -13 \times 10^4 \text{ km}^2 \text{ s}^{-2}$. These more loosely-bound retrograde stars are found to be on average more metal-poor, in agreement with e.g. Carollo et al. (2007). We find that over half of the identified substructures have $\sigma_{[\text{Fe}/\text{H}]} \leq 0.3$ dex, which is rather small given that the formal uncertainties of the individual star abundances in the RAVE data are ~ 0.25 dex. In fact, substructures VelHe1-4* and VelHe1-9* have $\sigma_{[\text{Fe}/\text{H}]} \leq 0.1$ dex, which makes them good candidates for being remnants of disrupted globular clusters.

We find all substructures, save for VelHe1-3*, to be α -enhanced in both Mg and Si as expected. In general, the α abundances of the stars in the substructures and in the retrograde halo component are consistent with the rest of the stars in our halo sample. This is also the case for their distribution in the space of $[\alpha/\text{Fe}]$ vs $[\text{Fe}/\text{H}]$, where the different substructures, with the exception of VelHe1-3*, follow the same trend as the rest of the halo sample.

We are clearly limited in our ability to understand the structures by the low number of stars with measured chemical abundances. This will change with the *Gaia* Data Release 2, that will certainly help us to better define the extent of the substructures in integrals of motion space, and to find more members. But more crucial are the upcoming spectroscopic surveys carried out by the new multi-object spectrographs WEAVE and 4MOST, which will be of great help in providing the data necessary to understand the nature and origin of these objects.

Acknowledgements. We gratefully acknowledge financial support from a VICI grant from the Netherlands Organisation for Scientific Research, NWO and from NOVA. This work has made use of data from the European Space Agency (ESA) mission *Gaia* (<http://www.cosmos.esa.int/gaia>), processed by the *Gaia* Data Processing and Analysis Consortium (DPAC, <http://www.cosmos.esa.int/web/gaia/dpac/consortium>). Funding for the DPAC has been provided by national institutions, in particular the institutions participating in the *Gaia* Multilateral Agreement. This work made use of *vaex* (Breddels & Veljanoski 2018), *numpy* (Walt et al. 2011), *matplotlib* (Hunter 2007), *scikit-learn* (Pedregosa et al. 2011), and *scikit-image* (van der Walt et al. 2014).

References

Belokurov, V., Zucker, D. B., Evans, N. W., et al. 2006, *ApJ*, 642, L137
 Bernard, E. J., Ferguson, A. M. N., Schlafly, E. F., et al. 2014, *MNRAS*, 443, L84
 Bernard, E. J., Ferguson, A. M. N., Schlafly, E. F., et al. 2016, *MNRAS*, 463, 1759
 Boeche, C., Siebert, A., Williams, M., et al. 2011, *AJ*, 142, 193
 Breddels, M. A. & Veljanoski, J. 2018, *ArXiv e-prints* [[arXiv:1801.02638](https://arxiv.org/abs/1801.02638)]
 Carollo, D., Beers, T. C., Chiba, M., et al. 2010, *ApJ*, 712, 692
 Carollo, D., Beers, T. C., Lee, Y. S., et al. 2007, *Nature*, 450, 1020
 Casey, A. R., Hawkins, K., Hogg, D. W., et al. 2017, *ApJ*, 840, 59
 Freeman, K. & Bland-Hawthorn, J. 2002, *ARA&A*, 40, 487
 Gaia Collaboration, Brown, A. G. A., Vallenari, A., et al. 2016, *A&A*, 595, A2
 Helmi, A. & de Zeeuw, P. T. 2000, *MNRAS*, 319, 657
 Helmi, A., Veljanoski, J., Breddels, M. A., Tian, H., & Sales, L. V. 2017, *A&A*, 598, A58
 Helmi, A. & White, S. D. M. 1999, *MNRAS*, 307, 495

Helmi, A., White, S. D. M., de Zeeuw, P. T., & Zhao, H. 1999, *Nature*, 402, 53
 Helmi, A., White, S. D. M., & Springel, V. 2003, *MNRAS*, 339, 834
 Hunter, J. D. 2007, *Computing In Science & Engineering*, 9, 90
 Kunder, A., Kordopatis, G., Steinmetz, M., et al. 2017, *AJ*, 153, 75
 Lindegren, L., Lammers, U., Bastian, U., et al. 2016, *A&A*, 595, A4
 McMillan, P. J., Kordopatis, G., Kunder, A., et al. 2017, *ArXiv e-prints* [[arXiv:1707.04554](https://arxiv.org/abs/1707.04554)]
 Nissen, P. E. & Schuster, W. J. 2010, *A&A*, 511, L10
 Pedregosa, F., Varoquaux, G., Gramfort, A., et al. 2011, *Journal of Machine Learning Research*, 12, 2825
 Tissera, P. B., Beers, T. C., Carollo, D., & Scannapieco, C. 2014, *MNRAS*, 439, 3128
 van der Walt, S., Schönberger, J. L., Nunez-Iglesias, J., et al. 2014, *PeerJ*, 2, e453
 Vincent, L. & Soille, P. 1991, *IEEE Trans. Pattern Anal. Mach. Intell.*, 13, 583
 Walt, S. v. d., Colbert, S. C., & Varoquaux, G. 2011, *Computing in Science and Engg.*, 13, 22
 Zolotov, A., Willman, B., Brooks, A. M., et al. 2009, *ApJ*, 702, 1058